SAND2015-9050J

Terahertz spaser radiating in a narrow beam

Chongzhao Wu,[1], Sudeep Khanal,[1] John L. Reno,[2] and Sushil Kumar[1]
[1]*Department of Electrical and Computer Engineering, Lehigh University, Bethlehem, PA 18015*
and
[2]*Sandia National Laboratories, Center of Integrated Nanotechnologies, MS 1303, Albuquerque, NM 87185-1303*

(Dated: July 6, 2015)

Spasers (plasmonic lasers) generate coherent surface-plasmon-polaritons (SPPs) and could be realized at subwavelength dimensions in metallic cavities for applications in nanoscale optics[1–4]. Plasmonic cavities are also utilized for terahertz quantum-cascade lasers (QCLs)[5,6], which are the brightest available solid-state sources of coherent terahertz radiation. A long standing challenge for all spasers demonstrated so-far is their poor coupling to far-field radiation. Unlike conventional lasers that could produce directional beams, spasers have highly divergent radiation patterns due to their subwavelength apertures. Here, we theoretically and experimentally demonstrate a new technique for implementing distributed-feedback (DFB) in spasers with Fabry-Pérot cavities, which is distinct from any other previously utilized DFB schemes for semiconductor lasers. The so-termed *antenna-feedback* scheme leads to single-mode operation in the spaser and couples the resonant SPP mode to a highly directional far-field radiation pattern. The narrow beam emission is due in part to the cavity acting like an end-fire phased-array antenna, as well as due to the large spatial extent of a coherent single-sided SPP mode that is excited on the metal film in the spaser's surrounding medium. Experimentally, the antenna-feedback method is implemented for terahertz QCLs, and single-mode terahertz QCLs with beam divergence as small as $4^\circ \times 4^\circ$ are demonstrated, which is significantly narrower than previously reported results[7,8]. Terahertz lasers with narrow-beam emission will find applications for integrated as well as standoff terahertz spectroscopy and sensing. The antenna-feedback scheme is generally applicable to any spaser with a Fabry-Pérot cavity irrespective of its operating wavelength, and could bring plasmonic nanolasers closer to practical applications.

Metallic cavities (or metallic nanoparticles[9]) supporting SPP modes have been used to realize nanoscale spasers for potential applications in integrated optics. Such cavities are also used for terahertz QCLs to achieve low-threshold and high-temperature performance[6]. The most common type of spasers with long-range SPPs, which include terahertz QCLs, utilize Fabry-Pérot type cavities in which at least one dimension is longer than the wavelength inside the dielectric[6,10–12]. A common challenge for all such spasers is the poor coupling of SPP modes in the cavity to free-space radiation, which results in highly divergent radiation and poor radiative efficiency. Periodic structures with broad-area emission are therefore used for narrow-beam emission[7,8,13,14]. However, Fabry-Pérot cavity structures with subwavelength apertures are more desirable, especially for electrically pumped spasers. The antenna-feedback method serves to couple the guided SPP mode in a spaser's cavity to a single-sided SPP mode that can exist in its surrounding medium by periodic perturbation of the metallic cladding in the cavity. This leads to excitation of coherent single-sided SPPs on the metallic cladding of the spaser, which couple to a narrow-beam in the far-field much like an end-fire phased-array antenna at the microwave frequencies[15].

Single-mode operation in spasers with Fabry-Pérot cavities could be implemented in a straightforward manner by periodically perturbing the metallic film that supports the resonant SPP modes. The schematic in Fig. 1(a) shows an example of a periodic grating in the top metal cladding for a parallel-plate metallic cavity that could be utilized to implement p-th order DFB by choosing the appropriate periodicity. Since the SPP mode has maximum amplitude at the interface of metal and dielectric active medium, a periodic perturbation in the metal film could provide strong Bragg diffraction up to high-orders for the counter-propagating SPP waves inside the active medium with incident and diffracted wavevectors k_i and $k_d = -k_i$ respectively, such that

$$k_i \;=\; p\frac{2\pi}{\Lambda} + k_d \qquad (1)$$

where Λ is the grating period, $2\pi/\Lambda$ is the grating wavevector, and p is an integer ($p = 1, 2, 3\ldots$) that specifies the diffraction order. For plane-wave like modes at frequencies far away from the plasma resonance in metal, $k_i \approx 2\pi n_\mathrm{a}/\lambda$, where λ is the free-space wavelength corresponding to the SPP mode and n_a is the effective propagation index in active medium (approximately the same as refractive index of the medium), the so-called Bragg

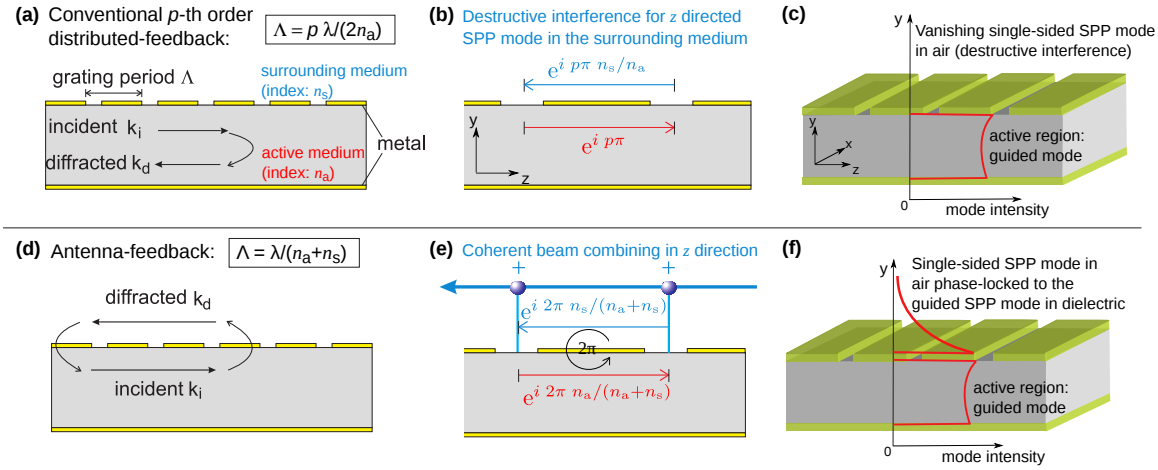

FIG. 1: **The antenna-feedback concept for spasers.** (a) The general principle of conventional distributed-feedback (DFB) that could be implemented in a spaser by introducing periodicity in its metallic cladding. A parallel-plate metallic cavity is illustrated; however, the principle is equally applicable to spaser cavities with a single metal-cladding. (b) If the periodicity in (a) is implemented by making holes or slits in the metal-cladding, the guided SPP wave diffracts out through the apertures and generates single-sided SPP waves on the cladding in the surrounding medium. The figure shows phase-mismatch between successive apertures for SPP waves on either side of the cladding. Coherent single-sided SPP waves in the surrounding medium cannot therefore be sustained owing to destructive interference with the guided SPP wave inside the cavity, as illustrated in (c). (d) Principle of an antenna-feedback grating. If the periodicity in the metal film allows the guided SPP mode to diffract outside the cavity, a grating period could be chosen that leads to the first-order Bragg diffraction in the opposite direction, but in the surrounding medium rather than inside the active medium itself. Similarly, the single-sided SPP mode in the surrounding medium undergoes first-order Bragg diffraction to couple with the guided SPP wave in the opposite direction inside the cavity. (e) The grating in (d) leads to a fixed phase-condition at each aperture between counter propagating SPP waves on the either side of metal-cladding. First, this leads to significant build up of amplitude in the single-sided SPP wave in the surrounding medium, as illustrated in (f). Second, emission from each aperture adds constructively to couple to far-field radiation in the end-fire (z) direction. As argued in the text, both of these aspects lead to narrow far-field emission profile in the $x-y$ plane.

mode with $\lambda = 2n_a\Lambda/p$ is resonantly excited because it is, by design, the lowest-loss mode in the DFB cavity within the gain spectrum of the active medium. For terahertz QCLs with metallic cavities, first-order[16] and second-order[17,18] DFBs have been implemented to achieve robust single-mode operation. However, these conventional DFB techniques do not achieve directionality of far-field radiation in both directions. Consequently, 2D photonic-crystal DFB structures have been utilized for broad-area (surface) single-mode emission[19,20] for which diffraction-limited beams could be achieved at the expense of large cavity dimensions.

In contrast to conventional DFB methods in which periodic gratings couple forward and backward propagating waves inside the active medium itself, the antenna-feedback scheme couples a single-sided SPP wave that travels in the surrounding medium with the SPP wave traveling inside the active medium as illustrated in Fig. 1(d). The SPP wave inside the active medium with incident wavevector $k_i \approx 2\pi n_a/\lambda$ is diffracted in the opposite direction in the surrounding medium with wavevector $k_d \approx -2\pi n_s/\lambda$. For the first-order diffraction grating ($p = 1$), equation (1) results in

$$\frac{2\pi n_a}{\lambda} = \frac{2\pi}{\Lambda} - \frac{2\pi n_s}{\lambda} \qquad (2)$$

that leads to excitation of a DFB mode with $\lambda = (n_a + n_s)\Lambda$, which is different from any of the p-th order DFB modes that occur at $\lambda = 2n_a\Lambda/p$. Hence, the antenna-feedback mode could always be excited by just selecting the appropriate grating period Λ such that the wavelength occurs close to the peak-gain wavelength in the active-medium. For GaAs/AlGaAs based terahertz QCLs, $n_a \sim 3.6$, $n_s = 1$, and hence for a chosen grating-period Λ, the first-order DFB, antenna-feedback, and second-order DFB modes occur at wavelengths 7.2 Λ, 4.6 Λ, and 3.6 Λ respectively. The typical gain-bandwidth of terahertz QCLs is less than 20% of the peak-gain wavelength, which suggests that the grating has to be designed specifically to excite the antenna-feedback mode.

The antenna-feedback scheme leads to excitation of a coherent single-sided SPP standing-wave on the metallic cladding of the spaser, which is phased-locked to the resonant-cavity SPP mode inside the active medium. Both waves maintain exact same phase relation at each aperture location, where they exchange electromagnetic (EM) energy with each other due to diffraction as illustrated in Fig. 1(e). The SPP wave in the surrounding medium is excited due to scattering of EM field at apertures that generates a combination of propagating quasi-cylindrical waves and SPPs[22,23] that propagate along the surface of the metal-film. The scattered waves thus generated at each aperture superimpose constructively in only the end-fire (z) direction owing to the phase-

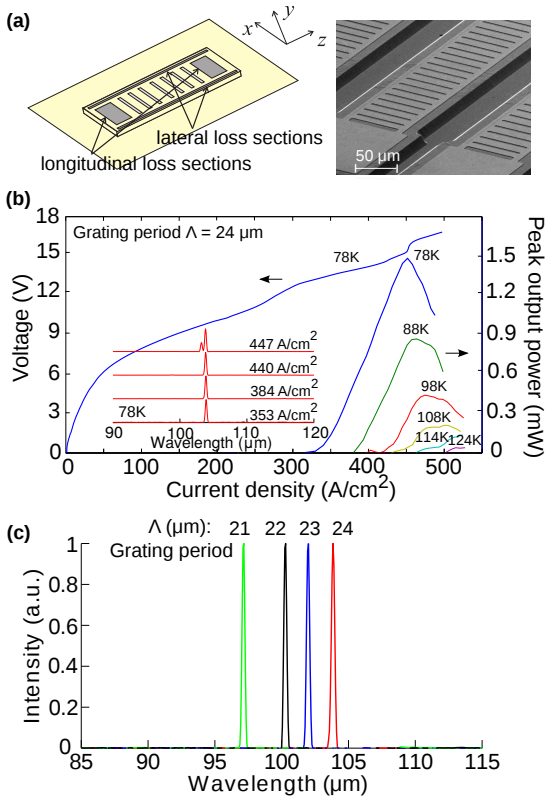

FIG. 2: **Lasing characteristics of terahertz QCLs with antenna-feedback.** (a) The schematic on left shows the QCL's metallic-cavity with antenna-feedback grating implemented in top metal cladding. The active-medium is 10 μm thick and based on a 3 THz GaAs/$Al_{0.10}Ga_{0.90}As$ QCL design[21]. A scanning-electron microscope image of the fabricated QCLs is shown on the right. (b) Experimental light-current-voltage characteristics of a representative QCL with antenna-feedback of dimensions 1.4 mm × 100 μm at different heat-sink temperatures. The QCL is biased with low duty-cycle current pulses of 200 ns duration and 100 kHz repetition rate. Inset shows lasing spectra for different bias where the spectral linewidth is limited by instrument's resolution. (c) Measured spectra for four different antenna-feedback QCLs with varying grating periods Λ, but similar overall cavity dimensions. The QCLs are biased at a current-density ∼ 440 A/cm^2 at 78 K.

condition thus established at each aperture. For coupling to far-field radiation, the radiation is therefore like that from an end-fire phased array antenna that produces a narrow beam in both x and y directions. For terahertz QCLs, this method is a significant improvement over the recently developed third-order DFB method for producing directional beams[24] that does not require any specific design considerations for phase-matching[25]. A comparison of antenna-feedback with third-order DFB for terahertz QCL cavities is presented in the supplementary section S3, where results from finite-element simulations (FEM) for the cavity eigenmodes are also presented.

Figure 2 shows experimental results from terahertz QCLs implemented with antenna-feedback gratings. Details about fabrication and measurement methods are presented in supplementary section S1. Fig. 2(b) shows representative L-I curves versus heat-sink temperature for a QCL with Λ = 24 μm. The QCL operated up to a temperature of 124 K. In comparison, multi-mode Fabry-Pérot cavity QCLs on the same chip that did not include longitudinal or lateral absorbing boundaries operated up to ∼ 140 K. The temperature degradation due to absorbing boundaries is relatively small and similar to previous reports of DFB terahertz QCLs[18]. The inset shows measured spectra at different bias at 78 K. Most QCLs tested with different grating periods showed robust single-mode operation except close to peak-bias when a second-mode was excited for some devices at a shorter-wavelength, which suggests it is likely due to a higher-order lateral model being excited due to spatial-hole burning in the cavity. Peak-power output of ∼ 1.5 mW was detected from the antenna-feedback QCL. For comparison, a terahertz QCL with third-order DFB and similar dimensions was also fabricated on the same chip, which operated up to a similar temperature of ∼ 124 K and emitted peak-power output of ∼ 0.45 mW (see section S3). The antenna-feedback gratings lead to greater radiative outcoupling compared to conventional DFB schemes for terahertz QCLs, which is discussed further in section S3.

Fig. 2(c) shows spectra measured from four different terahertz QCLs with antenna-feedback gratings of different grating periods Λ. The single-mode spectra scales linearly with Λ, which is the clearest proof that the feedback mechanism works as expected and the lower band-edge mode is selectively excited in each case. Using $\lambda = \Lambda(n_a + 1)$ from equation (2), the effective propagation index of the SPP mode in the active medium n_a is calculated as 3.6, 3.55, 3.46, and 3.38 for QCLs with Λ of 21 μm, 22 μm, 23 μm, and 24 μm respectively. The effective mode-index n_a decreases because a larger Λ introduces larger sized apertures in the metal film since the grating duty-cycle was kept same for all devices. Consequently, a greater amount of field couples to the single-sided SPP mode in air for increasing Λ, thereby reducing the modal confinement in the active medium that reduces the propagation index of the guided SPP mode further.

Experimental far-field beam patterns for antenna-feedback QCLs with varying designed parameters are shown in Fig. 3. Single-lobed beams in both lateral (x) and vertical (y) directions were measured for all QCLs. As shown in Fig. 3(b), the full-width half-maximum (FWHM) for the QCL with 70 μm width, Λ = 21 μm is ∼ 4° × 4°, which is the narrowest reported beam-profile from any terahertz QCL to-date. In contrast, previous schemes for emission in a narrow-beam have resulted in divergence angles of 6° × 11° using very long (> 5 mm) cavities and a phased-matched third-order DFB scheme[25] and 7° × 10° using broad-area devices with 2D photonic-crystals[20] for single-mode terahertz QCLs, and 4° × 10°[26] and 12° × 16°[27] for multi-mode QCLs using metamaterial collimators. Figs. 3(c) and 3(d) show representative beam patterns from QCLs with wider cavities of 100 μm width, for the smallest and largest Λ in the range of fab-

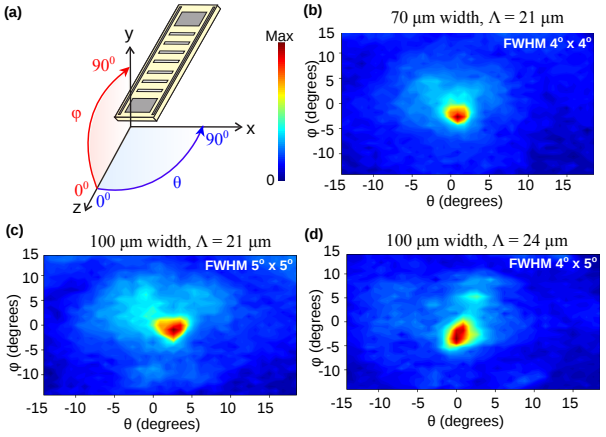

FIG. 3: **Far-field radiation-patterns of terahertz QCLs with antenna-feedback.** (a) Schematic showing orientation of QCLs and definition of angles. The QCLs were operated at 78 K in pulsed mode and biased at $\sim$ 440 A/cm^2 while lasing in single-mode. The plots are for QCLs with $\sim$ 1.4 mm long cavities and (b) 70 μm width and Λ = 21 μm grating emitting at $\sim$ 3.1 THz, (c) 100 μm width and Λ = 21 μm grating emitting at $\sim$ 3.1 THz, and (d) 100 μm width and Λ = 24 μm grating emitting at $\sim$ 2.9 THz respectively.

ricated devices respectively. The beam divergence is relatively independent of Λ as expected. More importantly, the measurements show that the wider cavities result in a slightly broader beam. Such a result is counter-intuitive because typically a laser emits in a narrower beam as its cavity's dimensions are increased due to an increase in the size of emitting aperture. Such a behavior is unique for a spaser with antenna-feedback, and is discussed along with full-wave 3D FEM simulation of the beam pattern in supplementary section S4. It can be argued that the size of the beam could be further narrowed by utilizing narrower cavities for terahertz QCLs, which will be extremely beneficial to develop cw sources of narrow-beam coherent terahertz radiation.

In conclusion, we have presented an antenna-feedback scheme to achieve single-mode operation and a highly directional far-field radiation pattern from spasers (plasmonic lasers) with subwavelength apertures and Fabry-Pérot type cavities. This can be achieved by perforating the metal film in the spaser with a periodic grating of holes or slits, which is relatively easy to implement for fabrication. The uniqueness of the method lies in the specific value of the grating's period, which leads to the spaser's cavity radiating like an end-fire phased-array antenna for the excited DFB mode. Additionally, coherent single-sided SPPs are also generated on the metal film that have a large spatial extent in the surrounding medium of the spaser's cavity, which could have important implications for applications in integrated plasmonics. Coherent SPPs with large spatial extent could make it easy to couple SPP waves from the spasers to other photonic components, and could also potentially be utilized for plasmonic sensing. Experimentally, the scheme is implemented in terahertz QCLs with metallic cavities. A beam-divergence angle as small as $4^\circ \times 4^\circ$ is achieved for single-mode QCLs, which is significantly narrower that that achieved with any other previously reported schemes for terahertz QCLs with periodic photonic structures. Terahertz QCLs with antenna-feedback could lead to development of new modalities for terahertz spectroscopic sensing and wavelength tunability due to access of a coherent terahertz SPP wave on top of the QCL's cavity, possibilities of sensing and imaging at standoff distances of few tens of meters, and development of integrated terahertz laser arrays with a broad spectral coverage for applications in terahertz absorption spectroscopy.

[1] D. J. Bergman and M. I. Stockman, "Surface plasmon amplification by stimulated emission of radiation: Quantum generation of coherent surface plasmons in nanosystems," *Phys. Rev. Lett.*, vol. 90, p. 027402, 2003.

[2] M. T. Hill and M. C. Gather, "Advances in small lasers," *Nat. Photon.*, vol. 8, p. 908, 2014.

[3] R. F. Oulton, "Surface plasmon lasers: sources of nanoscopic light," *Mater. Today*, vol. 15, p. 26, 2012.

[4] P. Berini and I. D. Leon, "Surface plasmon-polariton amplifiers and lasers," *Nat. Photon.*, vol. 6, p. 16, 2012.

[5] R. Köhler, A. Tredicucci, F. Beltram, H. E. Beere, E. H. Linfield, A. G. Davies, D. A. Ritchie, R. C. Iotti, and F. Rossi, "Terahertz semiconductor-heterostructure laser," *Nature*, vol. 417, pp. 156–159, 2002.

[6] B. S. Williams, "Terahertz quantum-cascade lasers," *Nat. Photon.*, vol. 1, pp. 517–525, 2007.

[7] L. Mahler and A. Tredicucci, "Photonic engineering of surface-emitting terahertz quantum cascade lasers," *Laser Photonics Rev.*, vol. 5, pp. 647–658, 2011.

[8] C. Sirtori, S. Barbieri, and R. Collombelli, "Wave engineering with thz quantum cascade lasers," *Nat. Photon.*, vol. 7, p. 691, 2013.

[9] M. A. Noginov, G. Zhu, A. M. Belgrave, R. Bakker, V. M. Shalaev, E. E. Narimanov, S. Stout, E. Herz, T. Suteewong, and U. Wiesner, "Demonstration of a spaser-based nanolaser," *Nature*, vol. 460, p. 1110, 2009.

[10] M. T. Hill, M. Marell, E. S. P. Leong, B. Smalbrugge, Y. Zhu, M. Sun, P. J. van Veldhoven, E. J. Geluk, F. Karouta, Y.-S. Oei, R. Nötzel, C.-Z. Ning, and M. K. Smit, "Lasing in metal-insulator-metal sub-wavelength plasmonic waveguides," *Opt. Express*, vol. 17, p. 11107, 2009.

[11] R. F. Oulton, V. J. Sorger, T. Zentgraf, R.-M. Ma, C. Gladden, L. Dai, G. Bartal, and X. Zhang, "Plasmon lasers at deep subwavelength scale," *Nature*, vol. 461, p. 629, 2009.

[12] Y.-J. Lu, J. Kim, H.-Y. Chen, C. Wu, N. Dabidian, C. E. Sanders, C.-Y. Wang, M.-Y. Lu, B.-H. Li, X. Qiu, W.-H. Chang, L.-J. Chen, G. Shvets, C.-K. Shih, and S. Gwo, "Plasmonic nanolaser using epitaxially grown silver film," *Science*, vol. 337, p. 450, 2012.

[13] W. Zhou, M. Dridi, J. Y. Suh, C. H. Kim, D. T. Co, M. R.

Wasielewski, G. C. Schatz, and T. W. Odom, "Lasing action in strongly coupled plasmonic nanocavity arrays," *Nat. Nanotech.*, vol. 8, p. 506, 2013.

[14] F. van Beijnum, P. J. van Veldhoven, E. J. Geluk, M. J. A. de Dood, G. W. t Hooft, and M. P. van Exter, "Surface plasmon lasing observed in metal hole arrays," *Phys. Rev. Lett.*, vol. 110, p. 206802, 2013.

[15] C. A. Balanis, *Antenna Theory: Analysis and Design*, 3rd ed. Wiley-Interscience, 2005.

[16] B. S. Williams, S. Kumar, Q. Hu, and J. L. Reno, "Distributed-feedback terahertz quantum-cascade lasers with laterally corrugated metal waveguides," *Opt. Lett.*, vol. 30, p. 2909, 2005.

[17] J. A. Fan, M. A. Belkin, F. Capasso, S. Khanna, M. Lachab, A. G. Davies, and E. H. Linfield, "Surface emitting terahertz quantum cascade laser with a double-metal waveguide," *Opt. Express*, vol. 14, p. 11672, 2007.

[18] S. Kumar, B. S. Williams, Q. Qin, A. W. M. Lee, Q. Hu, and J. L. Reno, "Surface-emitting distributed feedback terahertz quantum-cascade lasers in metal-metal waveguides," *Opt. Express*, vol. 15, p. 113, 2007.

[19] Y. Chassagneux, R. Colombelli, W. Maineult, S. Barbieri, H. E. Beere, D. A. Ritchie, S. P. Khanna, E. H. Linfield, and A. G. Davies, "Electrically pumped photonic-crystal terahertz lasers controlled by boundary conditions," *Nature*, vol. 457, p. 174, 2009.

[20] Y. Halioua, G. Xu, S. Moumdji, L. H. Li, A. G. Davies, E. H. Linfield, and R. Colombelli, "THz quantum cascade lasers operating on the radiative modes of a 2D photonic crystal," *Opt. Lett.*, vol. 39, p. 3962, 2014.

[21] S. Khanal, L. Zhao, J. L. Reno, and S. Kumar, "Temperature performance of terahertz quantum-cascade lasers with resonant phonon active-regions," *J. Opt*, vol. 16, p. 094001, 2014.

[22] P. Lalanne, J. Hugonin, H. Liu, and B. Wang, "A microscopic view of the electromagnetic properties of sub-λ metallic surfaces," *Surf. Sci. Rep.*, vol. 64, p. 453, 2009.

[23] A. Babuty, A. Bousseksou, J.-P. Tetienne, I. M. Doyen, C. Sirtori, G. Beaudoin, I. Sagnes, Y. D. Wilde, and R. Colombelli, "Semiconductor surface plasmon sources," *Phys. Rev. Lett.*, vol. 104, p. 226806, 2010.

[24] M. I. Amanti, M. Fischer, G. Scalari, M. Beck, and J. Faist, "Low-divergence single-mode terahertz quantum cascade laser," *Nat. Photon.*, vol. 3, pp. 586–590, 2009.

[25] T. Y. Kao, Q. Hu, and J. L. Reno, "Perfectly phase-matched third-order DFB THz quantum-cascade lasers," *Opt. Lett.*, vol. 37, p. 2070, 2012.

[26] G. Liang, E. Dupont, S. Fathololoumi, Z. R. Wasilewski, D. Ban, H. K. Liang, Y. Zhang, S. F. Yu, L. H. Li, A. G. Davies, E. H. Linfield, H. C. Liu, and Q. J. Wang, "Planar integrated metasurfaces for highly-collimated terahertz quantum cascade lasers," *Sci. Rep.*, vol. 4, p. 7083, 2014.

[27] N. Yu, Q. J. Wang, M. A. Kats, J. A. Fan, S. P. Khanna, L. Li, A. G. Davies, E. H. Linfield, and F. Capasso, "Designer spoof surface plasmon structures collimate terahertz laser beams," *Nat. Materials*, vol. 9, p. 730, 2010.

[28] O. Demichel, L. Mahler, T. Losco, C. Mauro, R. Green, A. Tredicucci, J. Xu, F. Beltram, H. E. Beere, D. A. Ritchie, and V. Tamošinuas, "Surface plasmon photonic structures in terahertz quantum cascade lasers," *Opt. Express*, vol. 14, p. 5335, 2006.

[29] COMSOL 4.4, a finite-element partial differential equation solver from COMSOL Inc.

Acknowledgments

This work is supported by the U.S. National Science Foundation under Grant Nos. ECCS 1128562 and ECCS 1351142. It is performed, in part, at the Center for Integrated Nanotechnologies, a U.S. Department of Energy (DOE), Office of Basic Energy Sciences user facility. Sandia National Laboratories is a multiprogram laboratory managed and operated by Sandia Corporation, a wholly owned subsidiary of Lockheed Martin Corporation, for the U.S. DOE's National Nuclear Security Administration under contract DE-AC04-94AL85000.

Terahertz spaser radiating in a narrow beam
C. Wu *et al.*

Supplementary Information

S1. Fabrication and measurement details

The active-medium of the QCLs is based on a three-well resonant-phonon design with GaAs/$Al_{0.10}Ga_{0.90}As$ superlattice (design RTRP3W197), which is described in Ref. 21, and was grown by molecular-beam epitaxy. The QCL superlattice is 10 μm thick with an average n-doping of 5.5×10^{15} cm^{-3}, and surrounded by 0.05 μm and 0.1 μm thick highly-doped GaAs contact layers at 5×10^{18} cm^{-3} on either side of the superlattice. Fabrication of QCLs with parallel-plate metallic cavities followed a Cu-Cu thermocompression wafer bonding technique as in Ref. 18 with standard optical contact lithography. Following wafer-bonding, the 0.1 μm thick highly-doped GaAs layer (which lies below the top metal cladding after final fabrication) was selectively left exposed to realize 10 μm wide absorbing boundaries at both longitudinal and lateral edges of the QCL cavity as illustrated in Fig. 2(a) using positive-resist lithography. The absorbing boundaries result in a highly lossy propagation of the SPP modes in those regions[28]. While the longitudinal boundaries help in DFB mode discrimination, the lateral boundaries are useful to eliminate higher order lateral SPP modes by making them more lossy[18,19]. Ti/Au metal layers of thickness 25/200 nm were used as the top metal cladding, using an image-reversal lithography mask for implementing gratings in the metal layers. A third positive-resist lithography step was used to cover the grating-metal with photoresist to be used as a mask for wet-etching of ridges in a H_2SO_4:H_2O_2:H_2O 1:8:80 solution for $\sim$ 22 minutes. After etching the 10 μm thick superlattice active region when the bottom metal layer is exposed, an over-etch of $\sim$ 1 minute is followed up to reduce the slope on the sidewalls of the QCL's cavities to allow for a more uniform current-density distribution through the height of the cavity (in y direction). A Ti/Au contact was used as the backside-metal contact for the finally fabricated QCL chips to assist in soldering. Before deposition of backside-metal of the wafer, the substrate was mechanically polished down to a thickness of 170 μm to improve heat-sinking.

A cleaved chip consisting of QCLs with antenna-feedback gratings of different periods along with some Fabry-Pérot ridge QCLs and third-order DFB QCLs was then In-soldered on a Cu block, the QCL to be tested was wire-bonded for electrical biasing, and the Cu block was mounted on the cold-stage of a liquid Nitrogen vacuum cryostat for measurements. The emitted optical power is measured with a deuterated triglycine sulfate pyroelectric detector (DTGS) pyroelectric detector and calibrated with a terahertz thermopile powermeter (Scien-Tech model AC2500H) without any optical component or cone collecting optic inside the cryostat to improve collection of radiated power. The spectra were measured at 78 K in linear-scan mode with a resolution of 0.2 cm^{-1} (6 GHz) using a Bruker Fourier-transform infrared spectrometer (FTIR) under vacuum, with a room-temperature DTGS detector placed inside the FTIR. Far-field radiation patterns were measured with a DTGS pyroelectric cell detector mounted on a computer-controlled two-axis ($x - y$ plane) moving stage in the end-fire (z) direction at a distance of 65 mm from the QCLs' end-facets. The detector's size leads to spatial averaging of the measured beam with a step-size of 1.7°, which has a negligible impact on the measured beam-width.

S2. Modeling

Finite-element (FEM) simulations were performed using a commercially available software[29]. The eigenmodes of the DFB cavities are computed using an eigenfrequency solver. The loss in absorbing boundaries of the cavity is implemented using a complex dielectric constant computed using Drude-model[18]. The imaginary part of the computed eigenfrequencies is used to compute the propagation loss of the resonant-cavity modes in the units of inverse of length. The active region and the metal layers are modeled as lossless, in which case, the computed loss is the sum of loss at absorbing boundaries as well as that due to radiation (outcoupling). The shapes of the eigenmodes as well as eigenmode spectrum does not change if the active region and metal layers are made lossy. For the 2D simulations (cavities of infinite-width) the far-field boundaries are modeled as absorbing layers as described in Ref. 18. For 3D simulations, the in-built perfectly matched layers in the FEM solver were utilized to model the far-field boundaries.

S3. Comparison of antenna-feedback with third-order DFB

A third-order DFB technique was recently shown to achieve emission in a narrow beam for terahertz QCLs with Fabry-Pérot cavities[24]. It can achieve high directionality for the radiated beam in both directions perpendicular to propagation, so long as the effective propagation index of the SPP wave inside the active medium could be made $\sim$ 3.0. The so-called phase matching condition is possible for GaAs-based QCLs by cavity engineering[25] since the $n_{\mathrm{GaAs}} \sim 3.6$ is close to 3.0. The antenna-feedback technique in this work offers similar outcome as a perfectly matched third-order DFB with significantly improved directionality as well as better outcoupling efficiency of the radiated beam from terahertz QCLs. It is to be noted that the antenna-feedback scheme is automatically phase-matched and hence it could be utilized for any type of spaser without any restrictions on the required index in the active medium.

Figure S1 shows comparison of the eigenmode spec-

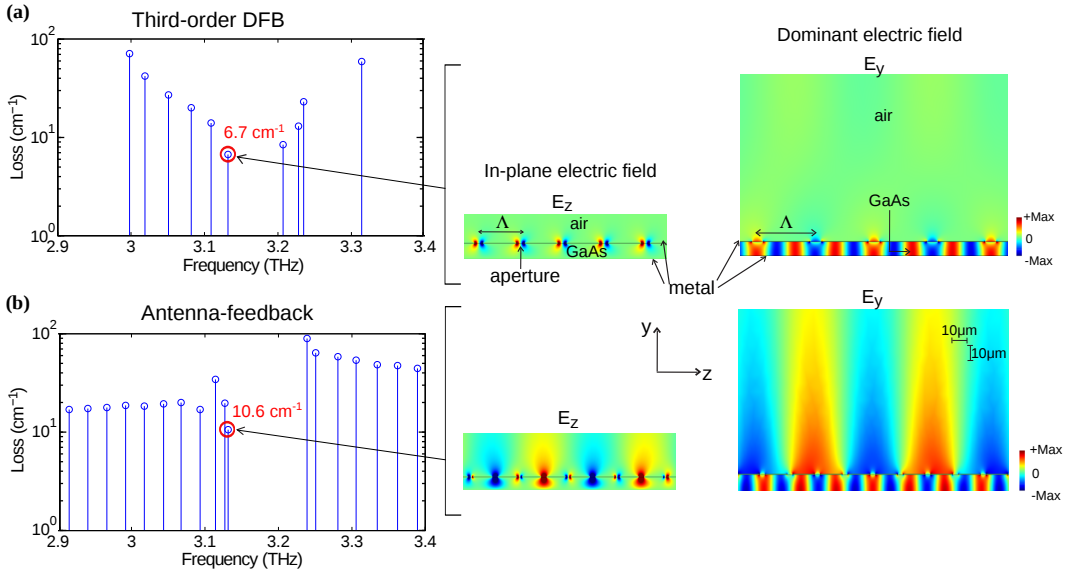

FIG. S1: **Comparison between third-order DFB and antenna-feedback schemes for terahertz QCL cavities.** The figure shows SPP eigenmode spectrum and electric-field for the eigenmode with lowest loss calculated by finite-element simulations of parallel-plate metallic cavities as in Fig. 1, with GaAs as dielectric ($n_a = 3.6$) and air as surrounding medium ($n_s = 1$). Simulations are done in 2-D (i. e. cavities of infinite-width) for 10 μm thick and 1.4 mm long cavities, and metal and active-layers are considered lossless. Lossy sections are implemented in the cavities at both longitudinal ends of the cavity to implement absorbing boundaries[28], which eliminates reflection of guided SPP modes from the end-facets. A periodic grating with apertures of (somewhat arbitrary) width 0.2Λ in the top-metal cladding are implemented for DFB. Λ is chosen to excite the lowest-loss DFB mode at similar frequencies close to ~ 3 THz. The eigenmode spectrum shows frequencies and loss for the resonant-cavity modes, which reflects combination of radiation loss and the loss at longitudinal absorbing regions. Fig. (a) shows results from a third-order DFB grating with $\Lambda = 41.7$ μm and (b) shows results from antenna-feedback grating with $\Lambda = 21.7$ μm. Radiation loss occurs through diffraction from apertures, and the amplitude of in-plane electric-field E_z is indicative of the outcoupling efficiency. The major fraction of EM energy for the resonant modes exists in TM polarized (E_y) electric-field. A photonic bandgap in the eigenmode spectrum is indicative of DFB effect due to the grating. The antenna-DFB grating excites a strong single-sided SPP standing-wave on top of the metallic grating (in air) as also illustrated in Fig. 1(f). Also, the radiative loss for the third-order DFB grating is smaller since the lowest-loss eigenmode has zeros of E_z under the apertures, which leads to smaller net outcoupling of radiation.

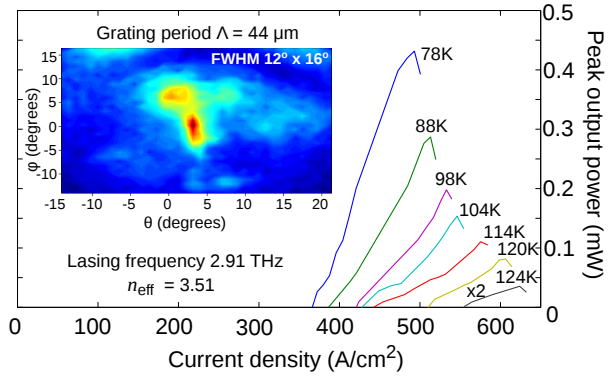

FIG. S2: **Lasing characteristics of a terahertz QCL with third-order DFB.** Light-current characteristics of a terahertz QCL with third-order DFB with similar cavity dimensions and fabrication sequence as the terahertz QCLs with antenna-feedback for which data is presented in Fig. 2. The inset shows the measured far-field radiation-pattern with the same angular definitions as in Fig. 3(a). The QCL emitted predominantly in single-mode at $\lambda = 103.0$ μm ($\nu = 2.91$ THz). Measured spectra for the device are not shown.

trum of a terahertz QCL cavity with third-order DFB versus antenna-feedback gratings computed using a finite-element solver[29]. The occurrence of band-gaps in the spectra is indicative of the DFB effect. In both cases, the lower-frequency band-edge mode is the lowest-loss mode by way of DFB action, since the DFB modes result in a standing-wave being established along the length of the cavity with an envelope shape that vanishes close to the longitudinal boundaries (end-facets). For antenna-feedback grating, a standing-wave for the single-sided SPP wave is additionally established in air, as can be seen from the field-plot of the band-edge mode in Fig. S1(b). In contrast, third-order DFB leads to negligible amplitude of the single-sided SPP wave in air, as mentioned previously and illustrated schematically in Fig. 1(c). The absorbing boundaries at the longitudinal ends of the cavity[28] increase the relative loss of the modes that are further away from the band-edge mode, which helps in mode discrimination and will lead to excitation of the desired band-edge mode for single-mode operation of the spaser. For the band-edge modes in Fig. S1(a) and Fig. S1(b), a loss of ~ 5 cm^{-1} was estimated as a contribution

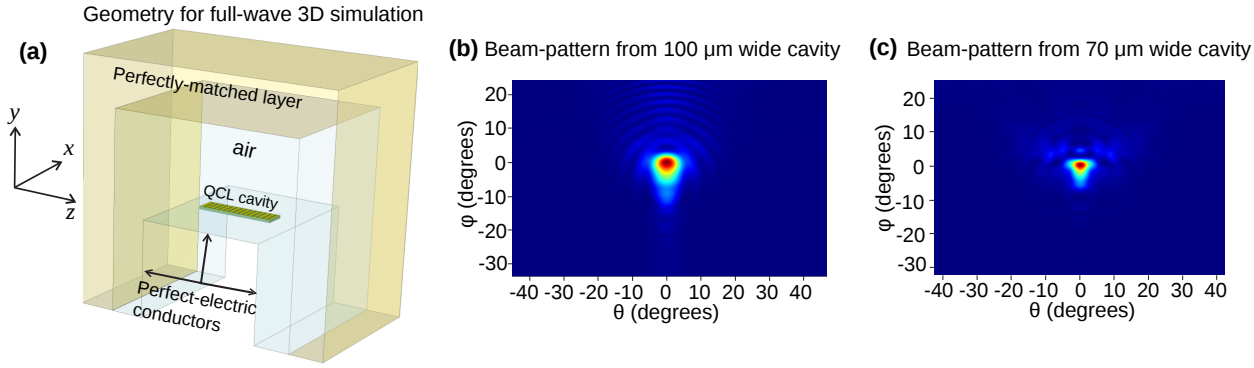

FIG. S3: **Full-wave 3D simulation to compute far-field radiation pattern of QCL cavities with antenna-feedback.** (a) The modeled geometry for full-wave 3D simulation with the FEM solver[29]. Parallel-plate metallic terahertz QCL cavities of 1.4 mm length, 10 μm thickness, varying widths, and a grating period of $\Lambda = 21.7$ μm were implemented, which excite antenna-feedback resonant-cavity modes at $\nu \sim 3.1$ THz. (b) Simulated far-field radiation pattern of the cavity with 100 μm width. The FWHM is $\sim 7^\circ \times 7^\circ$. (c) Far-field radiation pattern of the cavity with 70 μm width. The FWHM is $\sim 6^\circ \times 5^\circ$.

from the absorbing boundaries. Consequently, the radiative (outcoupling) loss of of the third-order DFB is ~ 1.7 cm^{-1} as compared to ~ 5.6 cm^{-1} for the antenna-feedback. The radiative loss of the third-order DFB is smaller since the band-edge mode has zeros of the radiative field (E_z) being located at each aperture, since the grating period Λ is integer multiple of half-wavelengths in the GaAs/AlGaAs active medium ($\Lambda = 3\lambda_{\mathrm{GaAs}}/2$, where $\lambda_{\mathrm{GaAs}} \equiv \lambda/n_{\mathrm{GaAs}}$). Such a low-outcoupling efficiency is also existent in surface-emitting terahertz QCLs with second-order DFB[18]. For the cavity with antenna-feedback, the radiative loss is higher because the grating period is not an integer multiple of half-wavelengths inside the active medium ($\Lambda \sim 0.78\lambda_{\mathrm{GaAs}}$) that leads to large amplitudes of the radiative-field (E_z) in alternating apertures as shown in the figure. As a consequence, the output power from terahertz QCLs with antenna-feedback should be greater than that with third-order DFB gratings, which is an additional advantage of the antenna-feedback scheme for terahertz QCLs. This was also verified experimentally as described in the following paragraph.

Figure S2 shows L-I characteristics of a representative terahertz QCL with third-order DFB that was fabricated on the same chip, and with similar dimensions as that of the antenna-feedback QCLs whose data is reported in Fig. 2. Using the phase condition $\lambda = 2n_{\mathrm{a}}\Lambda/p$ as determined from equation (1) for $p = 3$ (third-order DFB), an effective-mode index of $n_{\mathrm{a}} = 3.51$ is estimated for the resonant-cavity SPP mode in the active medium of the cavity. For ideal phase-matching, a mode-index value of 3.0 is required, hence the phased-matching condition is not satisfied for this QCL. Consequently, the measured FWHM of the far-field radiation pattern $\sim 12^\circ \times 16^\circ$ for this QCL is not as good as that for phased-matched third-order DFB QCLs[25]. The peak output peak power for the QCL is ~ 0.45 mW at 78 K, which is about three times less than that obtained for the antenna-feedback QCL with similar dimensions. However, this result is expected from the radiative losses estimated via 2D FEM simulations for similar cavity dimensions, which also scale in a similar manner as shown in Fig. S1. The maximum operating temperature of this QCL is almost similar to that of the antenna-feedback QCL, which suggests that radiative loss is relatively a small fraction of the overall waveguide loss in both types of DFB QCL cavities. This also suggests that there is a scope for enhancing radiative efficiency to increase optical power output without causing a significant degradation in temperature performance of terahertz QCLs with antenna-feedback.

S4. Full-wave 3D simulation for radiation-patterns

The narrow-beam emission from spasers with antenna-feedback is due to a combination of two factors that are related to the radiative behavior of phased-array antennas. In addition to the *array-factor* that leads to narrower beams for more number of elements in a phased-array (i. e. in this case, a longer length of the spaser's cavity), the far-field radiation pattern is additionally narrowed owing to an *element-factor*, which is defined as the far-field radiation pattern due to an individual emitter of the phased-array[15]. The large spatial extent of the single-sided SPP wave in the surrounding medium results in a narrower element-factor compared to an omnidirectional point-source emitter.

As measured experimentally and shown in Fig. 3, the antenna-feedback terahertz QCL cavities with a narrower width of 70 μm resulted in a beam with smaller divergence as compared to the 100 μm wide cavity. This seemingly unique behavior from antenna-feedback QCLs serves to further validate the concept of the specific feedback scheme, in which the cavity radiates like a phased-array antenna. A narrower cavity causes greater lateral spread of the single-sided SPP mode (in the x dimension) in the surrounding medium, especially when the cavity's width is sub-wavelength. A single-sided SPP mode with

a broader cross-section in the $x-y$ plane will lead to a more directional far-field radiation pattern owing to a narrower element-factor for the phased-array antenna structure.

To further validate the experimental results of Fig. 3, full-wave 3D FEM simulations were carried out for terahertz QCL cavities with antenna-feedback. Figure S3 shows the computed far-field radiation patterns for band-edge DFB mode for terahertz QCL cavities implemented with antenna-feedback gratings in the top metal cladding. The in-built perfectly-matched layers (PMLs) in the FEM solver[29] serve as an effective absorbing boundary for computation of the radiation pattern. The PMLs' parameters are coarsely adjusted to achieve minimum reflection at terahertz frequencies and transform the propagating waves to exponentially decaying waves. The PMLs are placed far enough to avoid interaction with the single-side SPP standing-wave in the near-field of the cavity. Considering the computer's memory limitations, laterally absorbing boundaries are not modeled in the cavity, which does not impact the simulation's results since the DFB mode could always be found, even though it is not the lowest loss mode in the eigenmode spectrum of the cavity due to other higher order lateral modes that can have even lower propagation loss. All metal layers are modeled as perfectly conducting surfaces to limit the mesh size in the geometry. In order to set up a far-field calculation, a far-field domain node is implemented that is a single closed surface surrounding all radiating apertures in the cavity. The distribution of far EM field is based on the Fourier transform of the near-field as implemented in the FEM solver. Simulated 3D beam patterns demonstrate single-lobed beams with narrow divergence for the band-edge mode with antenna-feedback as shown in the figure. The shape and FWHM of the computed radiation-pattern is in close agreement with the experimentally measured beams that are shown in Fig. 3. The FWHM of simulated beam patterns is slightly larger than that of the measured results. The difference are likely due to the relative simplification of implemented 3D model, which does not account for the sloped sidewall profile of the ridges and also the fact the ground plane around the QCL's cavity is different for the measured chip as compared to that in the simulated geometry.